

Chapter 2

Subsurface Characterization of Heat Treated Subtractive and Additive Manufactured (SLM) Ti6Al4V Specimens



Sangeeth Suresh, Ruganethan Sandarsekran, Mohd Zaid Abu Yazid, and Darulihsan Abdul Hamid

Abstract The widespread use of additive manufacturing (AM) for Ti6Al4V components have demanded an equally extensive study on their comparison with the subtractive manufactured counterparts. Subtractive manufacturing (SM) of Ti6Al4V has its own limitations due to the peculiar properties of the material in the rolled condition. AM process too has its own set of limitations that include porosity, brittleness, and high residual stresses leading to premature failure. Heat treatment (HT) is an option to counter these drawbacks to a certain extent. This study analyzes the effects of HT on the mechanical properties, surface and subsurface characteristics of both AM and SM specimens. A stress relieving process followed by HT above β transus temperature and an aging process enhances the hardness in both counterparts. However, surface levels of SM specimens prove better than AM specimens for wear-resistant applications. AM specimens require the removal of surface to depths between 100 and 200 μm to act as a wear-resistant surface. AM specimens attain a β phase prior to HT and hence a stress relieving operation would suffice in case its being used for applications that require a tough core.

Keywords Ti6Al4V · SLM printing · HT · Subsurface · Microstructure

S. Suresh (✉) · R. Sandarsekran · M. Z. A. Yazid · D. A. Hamid
Univeristi Kuala Lumpur-Malaysia Italy Design Institute, Cheras, Kuala Lumpur, Malaysia
e-mail: sangeeth@unikl.edu.my

R. Sandarsekran
e-mail: ruganethan.sandarsekran@s.unikl.edu.my

M. Z. A. Yazid
e-mail: mzaiday@unikl.edu.my

D. A. Hamid
e-mail: darulihsan@unikl.edu.my

2.1 Introduction

The use of titanium grade 5 alloy (Ti6Al4V) as a replacement for heavier metals in various automotive, aerospace, marine, medical, and other applications is widely attributed to its significant mechanical properties, including its high strength to weight ratio, resistance to wear and corrosion, high hardness, and excellent workability in high temperatures [1]. The characteristics that make Ti6Al4V a difficult-to-machine material are, its low thermal conductivity that accumulates heat at the machined surface causing variations in the surface properties, its high hardness that reduces tool life and causes strain hardening, its chemical reactivity causing rapid deterioration of the coatings on the cutting tools [2, 3]. Products built through an AM process could vary in volume from its SM counterpart slightly due to unavoidable porosities and inhomogeneities that could eventually affect their mechanical properties [4, 5]. A comparison between the SM and AM methods is shown in Fig. 2.1. This study focusses on the selective laser melting AM process as depicted in Fig. 2.2, in which the laser beam heats up the powder particles till they melt and bond with each other [6].

Major drawbacks with the SM process are the enormous wastage of material and limitations in terms of intricate and hidden geometries that cannot be machined [7–9]. Residual stress is yet another factor to be considered both in the SM and the AM methods, because of the influence of thermal energy in both the processes. In AM, the temperature gradients are produced by the laser beam. In such cases a martensitic alteration is necessary in the form of a stress relieving operation [10]. Further HT and aging processes have been recommended for both SM and AM components to enhance the hardness and wear resistance of the components. The β transus temperature (996 °C) is defined as the temperature at which the α phase of Ti6Al4V converts into a β phase with a proportional crystalline structural transformation from a hexagonal close packed (hcp) to a body centered cubic (bcc) structure causing increase in hardness [11]. Surface distortions as shown in Fig. 2.3, and stress accumulation in the machined specimens, both the AM and the SM counterparts, warrant further HT processes to enhance the lost surface and bulk properties [12–14]. This study delves into the optimization of HT parameters to measure the microhardness and

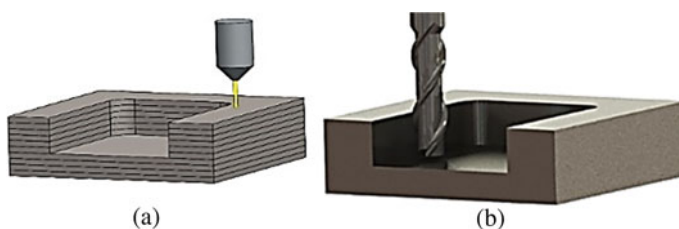


Fig. 2.1 a SLM printing in layers (CAD); b post-printing-layers fused together; c raw material for SM; d SM—milling process

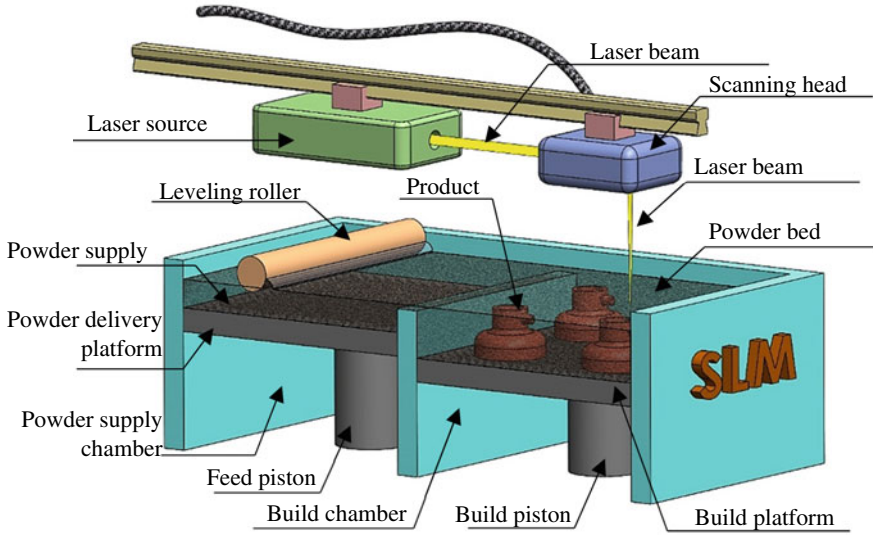


Fig. 2.2 SLM AM process with powder feedstock

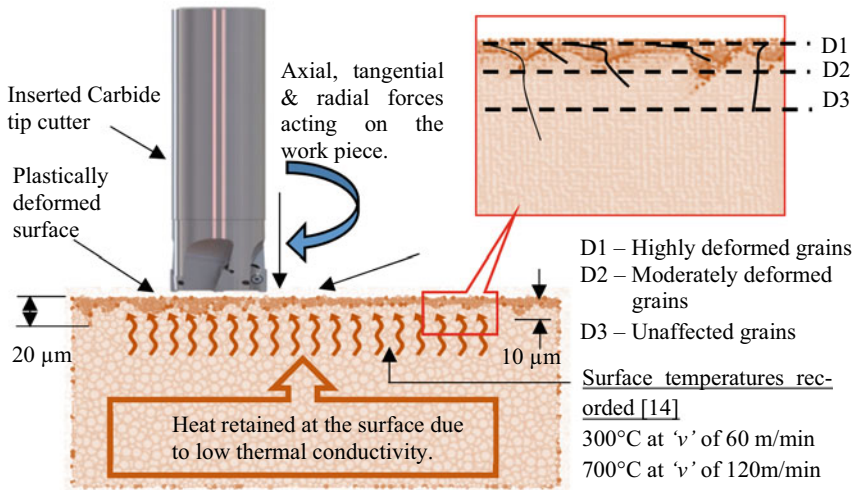


Fig. 2.3 Surface deformations observed in machining of Ti6Al4V

microstructure of both the SM and AM variants, at surface and subsurface levels paving groundwork for further tribological analysis.

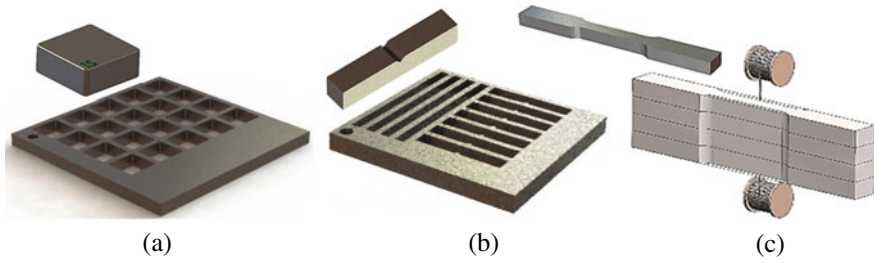


Fig. 2.4 EDM wire-cut of **a** surface characterization and tribo-test specimens, **b** tensile and Charpy specimens, **c** tensile stack wire-cut

2.2 Methodology

2.2.1 Milling Process (*Subtractive Manufacturing—SM*)

The milling process is carried out on a DMU 50 series three-axis machine. The cutting speed (v) is kept at a magnitude of 60 m/min (chosen to avoid overheating and adhesions at higher cutting speeds [15]), resulting in a spindle speed of 765 RPM for a $\text{\O}25$ mm two-tipped inserted cutter, using carbide inserts PVD coated with a TiN-TiAlN coating (85 HRC). A Sumitomo-AXMT170508PEER-E tip with a tip radius and a relief angle of R0.8 mm and 11° is used with a feed rate (f) rounded off to 200 mm/min at a chip load of 0.125 mm/tooth. The specimen size of $100 \times 100 \times 10$ mm is reduced to 6 mm (2 mm depth of cut per side) thickness. A volumetric removal of $20,000 \text{ mm}^3$ is facilitated in each of the two cuts to induce residual stress and evaluate post-machining surface alterations. Similar arrangement is carried out for the tensile and Charpy specimens. After milling the specimens for the respective tests are cut out using a wire cut EDM machine as shown in Fig. 2.4.

2.2.2 Selective Laser Melting—SLM (*Additive Manufacturing*)

In the SLM process the interactivity between the powder stock material in the exposed layer and the laser beam transpires in microseconds wherein the powder stock melts and fuses with the immediate product layer below it. The SLM process is carried out on an SLM@ 280^{HL} which has a build chamber of $280 \times 280 \times 350$ mm with a dual laser system. With a build rate up to $55 \text{ cm}^3/\text{h}$, it can build a feature as thin as 0.15 mm at a scanning speed of 10 m/s. The Ti6Al4V powder particle size ranges from 20 to 63 μm . Inert argon gas inside the build chamber prevents oxidation on the specimens. The laser beam scans with a power of 275 W producing a heat of 2710 °K exceeding the melt temperatures of most metals and composites. This study uses the

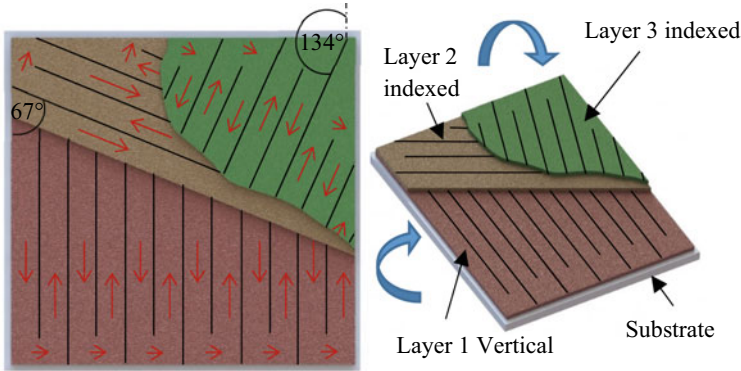


Fig. 2.5 Meander-path layer build up

meander scan path due to the small specimen size helping in a faster build rate and better homogeneity. The meander scan path starts with a vertical or horizontal path followed by a pre-programmed indexing to an angle of 67° in consecutive layers ($67^\circ, 134^\circ, 201^\circ \dots$ till the specimen height is achieved) as shown in Fig. 2.5 [16]. The process is carried out at a build speed of $15 \text{ cm}^3/\text{h}$ and a scanning speed of 700 mm/s . The thickness of the layer is $40 \text{ }\mu\text{m}$ and the spacing between the hatches is $60 \text{ }\mu\text{m}$. The laser power is maintained at 150 W . The laser beam diameter at the powder surface is $\text{Ø}0.20 \text{ mm}$.

2.2.3 Stress Relieving and HT—(SM and AM)

In milling (SM), the depth of cut is intentionally set to 2 mm per side to induce residual stresses and cause plastic deformation on the surface as shown in Fig. 2.3. Tool geometry and tool life are also major determinants of residual stresses in machined specimens [17]. At a constant depth of cut (a_p) of 5 mm , an increase in cutting speed (v) and feed rate (f) have shown a transformation from compressive to tensile stresses mainly noticed at subsurface levels of $10\text{--}20 \text{ }\mu\text{m}$. At lower subsurface levels negligible stresses have been observed. At lower cutting speeds (v) the tensile residual stress magnitudes of 520 MPa at the surface and compressive tensile stress of 300 MPa are recorded below the surface. However, as the cutting speed increases, only compressive stress magnitudes of $300\text{--}750 \text{ MPa}$ are observed, both, at the surface and below the surface, with no tensile stresses detected along the feed direction. A similar trend is also noticed in the cutting axis perpendicular to the feed direction. The residual stress values have been recorded at depths up to 0.08 mm [18]. Residual stresses within the specimens in SLM could result in deteriorated mechanical properties, cracks, and distortions as shown in Fig. 2.6. AM specimens have also recorded tensile stress of $100\text{--}300 \text{ MPa}$ at their surfaces and compressive stresses

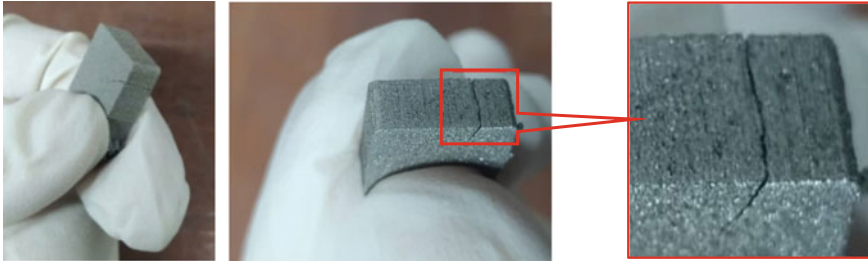


Fig. 2.6 Cracks formed in the specimens due to residual stresses in SLM

Table 2.1 HT experimental set up

Process	Temperature (°C)	Cooling method	Duration (h)
Hardening	950	Water Quenching	1
	1050	Air Cooling (220 m ³ /min approx.)	
	1150	Furnace Cooling	
Aging	500	Air Cooling (220 m ³ /min approx.)	4
	550		
	600		

of 38–80 MPa at the subsurface [19–22]. Since both processing methods exhibit almost similar residual stresses, the specimens from both processes are subjected to a constant stress relieving process in a HT furnace with optimized parameters, also to enhance its ductility [23]. The specimens are stress relieved through a cycle of heating processes in the furnace starting with a ramp up to 350 °C for a duration of one hour followed by a dwell period of 30 min at the same process. The second part of the cycle consists of a ramp up to 850 °C for a duration of one hour followed by furnace cooling. The stress relieving process is followed by a HT process to not only enhance the mechanical properties of the specimens but also regain their lost surface properties. An experimental design is adapted for HT, to validate the effects of heating above and below the β transus temperature of 995 °C. β transus temperature is the temperature above which phase changes are observed in the crystalline structure of Ti6Al4V specimens [24]. Optimization of the HT parameters is carried out in a Nabertherm N-11 h furnace. The preliminary experiment design is shown in Table 2.1. The hardness of the specimens is measured using a Highwood Digital Microhardness Tester.

2.2.4 Finishing Process

Surface characterization of specimens demands intensive surface finishing, starting with a surface grinding process. The depth of cut in grinding is maintained at 10 μ m

per cut (to avoid further buildup of residual stresses) at a cross feed of 0.5 m/min at a spindle speed of 3000 RPM under a water-soluble synthetic oil as cooling fluid. The grinding process is followed by polishing using emery sheets from a grit size of 600 for roughing to 2500 for a finish polishing operation, at a disk speed of 800 RPM. Polishing process is succeeded by an acetone immersion and ultra-sonic cleaning in distilled water to remove off any surface impurities. The specimens are chemical etched in Kroll's reagent (solution of water 93%, nitric acid 6%, and hydrofluoric acid 1%) to expose the surface for surface characterization.

2.2.5 Surface Characterization

Surface and subsurface microstructure is analyzed using optical microscope (Optika B600 MET) and scanning electron microscope (Hitachi SU1510 SEM). Surface composition and concentration of the alloying elements are inspected through an energy dispersive X-ray (Oxford Xplore 30 EDX) test.

2.3 Results and Discussion

The raw material hardness of SM specimens was 330 HV and the AM specimens at 360 HV. After the milling operation, no considerable variations in hardness have been observed. Stress relieving and further HT have shown the microhardness results to be favoring the combination of a hardening temperature of 1050 °C as represented in Table 2.2. The 10 μm depth is considered as the 'surface' here after the removal of HT scales. 100 and 200 μm are the subsurfaces. Post-heat treatment and the hardness of the AM specimens were observed to be higher than the SM counterparts in all the three temperature settings. The tensile strength of the AM specimens is almost the same regardless of the HT temperatures. The toughness of both variants at 1050 °C

Table 2.2 Microhardness values comparison between SM and AM specimens

Process	Hardening (60 min) + Water Quenching (°C)	Aging	HV at surface depth Z = – 10 μm	HV at surface depth Z = – 100 μm	HV at surface depth Z = – 200 μm
SM	950	500 °C (4 h) + Furnace cooling	392	455	404
	1050		553	497	469
	1150		410	461	427
AM	950		410	412	408
	1050		420	418	424
	1150		460	448	438

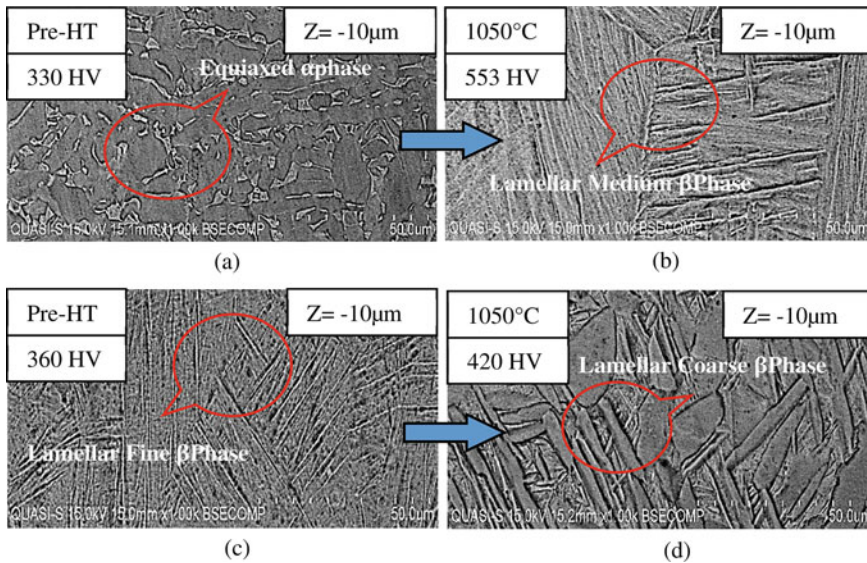


Fig. 2.7 Microstructural comparison 10 μm depth **a** SM-Pre-HT, **b** SM-Post-HT, **c** AM-Pre-HT, **d** AM-Post-HT

is better than at 1150 $^{\circ}\text{C}$. In the SM specimens, a transformation from the α phase to the β phase is observed, while in the AM specimens, both pre-HT and post-HT specimens exhibit a β phase as shown in Fig. 2.7. The obvious reason for this observation is the processing temperature. SM process has shown surface temperatures of 300–600 $^{\circ}\text{C}$ during the machining. These temperatures are still under the β transus temperature of 995 $^{\circ}\text{C}$ and hence cannot trigger a phase change. However, the process temperature of the AM process, at a laser power of 275 W peaks to as high as 2500 $^{\circ}\text{C}$ which is 2½ times greater than the β transus temperature. The AM (SLM) specimens can be seen dominated by the lamellar or columnar structures which represent a martensitic state with a BCC crystalline structure. Martensitic structures also exhibit higher tensile strength due to a higher hardness, but a lower ductility making it brittle [25]. A lamellar structure is also observed in the post-heat-treated SM specimens, which exhibit an obvious phase change from the initial equiaxed structure depicting a ferrite state with a BCC structure as seen in Fig. 2.7. The lamellar structure of the AM specimens transforms from fine to a coarse structure when heat treated. A coarser lamella indicates a more brittle surface prone to premature failure in applications characterized by frictional wear. In SM specimens medium grained lamellae are observed in the post-heat-treated SM specimens which indicates a less brittle surface. At the subsurface levels, finer lamellar grains are observed in both specimens indicating a less brittle surface which could be considered for applications requiring interaction between surfaces leading to a slower wear rate.

2.4 Conclusion

Applications of Ti6Al4V, as discussed earlier, ranges from wear-resistant functions like turbine blade disks, piston rings, etc., to functions that require high toughness like fasteners, connecting rods, springs, retainers, etc. Both SM and AM specimens exhibit different properties at different surface and subsurface levels. A higher hardness and tensile strength with a finer lamellar β phase surface would be appropriate for wear-resistant functions. For SM components, a fine lamellar surface is achieved through a HT above the β transus temperature (1050 °C) followed by a water quench and aging process to a temperature of 500 °C and furnace cooled. However, for AM specimens, the same set of HT processes followed by a surface removal to a depth between 100 and 200 μm either through a surface grinding, bead blasting or etching operation is recommended for wear-resistant surfaces. SM components do not have wear resistance requirements but need a tougher core could use an α phase HCP crystalline structure, which is obtained by HT below the β transus temperature (950 °C) followed by the same set of quenching and aging processes. This helps in retaining a tougher core. However, AM components develop a β phase BCC structure during the 3D printing stage itself due to the high temperature laser beam and hence retain the same crystalline structure. A stress relieving process on these components would be sufficient in applications that require a tougher core. Further study to analyze the wear resistance of the surface and the subsurface levels, their correlation to the surface microstructure, composition, and concentration of the alloying elements, will be studied through tribology experiments.

References

1. Liu C, Goel S, Llavori I, Stolf P, Giusca CL, Zabala A, Rabinovich GSF (2019) Benchmarking of several material constitutive models for tribology, wear, and other mechanical deformation simulations of Ti6Al4V. *J Mech Behav Biomed Mater* 97:126–137
2. Meilinger A, Torok I (2013) The importance of friction stir welding tool. *Prod Process Syst* 6(1):25–34
3. Liu S, Shin YC (2019) Additive manufacturing of Ti6Al4V alloy: a review, *Mater Des* 164:107552
4. Fan Z, Feng H (2018) Study on selective laser melting and HT of Ti-6Al-4V alloy. *Results Phys* 10:660–664
5. Huang R, Riddle M, Graziano D, Warren J, Das S, Nimbalkar S, Masanet E (2016) Energy and emissions saving potential of additive manufacturing: the case of lightweight aircraft components. *J Clean Prod* 135:1559–1570
6. Beretta S, Romano S (2017) A comparison of fatigue strength sensitivity to defects for materials manufactured by AM or traditional processes. *Int J Fatigue* 94:178–191
7. Patterson AE, Messimer SL, Farrington PA (2017) Overhanging features and the SLM/DMLS residual stresses problem: review and future research need. *Technologies* 5(2):15
8. Braian M, Jönsson D, Kevci M, Wennerberg A (2018) Geometrical accuracy of metallic objects produced with additive or subtractive manufacturing: a comparative in vitro study. *Dent Mater* 34(7):978–993

9. Suresh S, Abdul Hamid D, Yazid MZA, Che Daud NR, Mohd DNNL (2017) An investigation into the impact of flexural elastic modulus on the dimensional instability in CNC turning of titanium alloy grade 5-Ti6Al4V. *Mech. Eng. J.* 2:73–85
10. Suresh S, Hamid DA, Yazid MZA, Nasuha N, Ain SN (2017) Tool geometry and damage mechanisms influencing CNC turning efficiency of Ti6Al4V. *AIP Conf Proc* 1901(1):040004
11. Bejjani R, Bamford E, Cedergren S, Archenti A, Rashid A (2020) Variations in the surface integrity of Ti-6Al-4V by combinations of additive and subtractive manufacturing processes. *Materials* 13(8):1825
12. Khorasani AM, Gibson I, Ghaderi A, Mohammed MI (2019) Investigation on the effect of HT and process parameters on the tensile behaviour of SLM Ti-6Al-4V parts. *Int J Adv Manuf Technol* 101(9):3183–3197
13. Patil S, Jadhav S, Kekade S, Supare A, Powar A, Singh RKP (2016) The influence of cutting heat on the surface integrity during machining of titanium alloy Ti6Al4V. *Procedia Manuf.* 5:857–869
14. Sutter G, List G (2013) Very high-speed cutting of Ti–6Al–4V titanium alloy–change in morphology and mechanism of chip formation. *Int J Mach Tools Manuf* 66:37–43
15. Abdalla AO, Amrin A, Muhammad S, Hanim MA (2017) Effect of HT parameters on the microstructure and microhardness of Ti-6Al-4V alloy. *AIP Conf Proc* 1865(1):030001
16. Iqbal A, Suhaimi H, Zhao W, Jamil M, Nauman MM, He N, Zaini J (2020) Sustainable milling of Ti-6Al-4V: investigating the effects of milling orientation, cutter’s helix angle, and type of cryogenic coolant. *Metals* 10(2):258
17. Pitassi D, Savoia E, Fontanari V, Molinari A, Luchin V, Zappini G, Benedetti M (2018) Finite element thermal analysis of metal parts additively manufactured via selective laser melting. *Intech* 123–156
18. Shan C, Zhang M, Zhang S, Dang J (2020) Prediction of machining-induced residual stress in orthogonal cutting of Ti6Al4V. *Int J Adv Manuf Technol* 1–11
19. Yang D, Liu Z, Ren X, Zhuang P (2016) Hybrid modeling with finite element and statistical methods for residual stress prediction in peripheral milling of titanium alloy Ti-6Al-4V. *Int J Mech Sci* 108:29–38
20. Ahmad B, Van DVSO, Fitzpatrick ME, Guo H (2018) Residual stress evaluation in selective-laser-melting additively manufactured titanium (Ti-6Al-4V) and inconel 718 using the contour method and numerical simulation. *Addit Manuf* 22:571–582
21. Ali H, Ghadbeigi H, Mumtaz K (2018) Effect of scanning strategies on residual stress and mechanical properties of selective laser melted Ti6Al4V. *Mater Sci Eng A* 712:175–187
22. Ali H, Ghadbeigi H, Mumtaz K (2018) Processing parameter effects on residual stress and mechanical properties of selective laser melted Ti6Al4V. *J Mater Eng Perform* 27(8):4059–4068
23. Yang T, Liu T, Liao W, Zhang C, Duan S, Chen X (2018) Study on deformation behavior of Ti6Al4V Parts fabricated by selective laser melting. *MATEC Web Conf.* 237:01008
24. Khorasani AM, Ian G, Moshe G, Guy L (2018) A comprehensive study on surface quality in 5-axis milling of SLM Ti-6Al-4V spherical components. *Int J Adv Manuf Technol* 94(9):3765–3784
25. Pilchak AL, Sargent GA, Semiatin SL (2018) Early stages of microstructure and texture evolution during beta annealing of Ti-6Al-4V. *Metall Mater Trans A Phys Metall Mater Sci* 49(3):908–919